LUXE Technical Note

Electromagnetic calorimeter

Authors:

Faculty of Physics and Applied Computer Science, AGH University of Science and Technology, Krakow, Poland
M. Firlej, T. Fiutowski, M. Idzik, J. Moroń and K. Świentek

Deutsches Elektronen Synchrotron, Hamburg and Zeuthen, Germany
A. Borysov, M. Borysova, L. Helary and W. Lohmann[1]

Institute for Space Science, Bucharest, Romania
V. Ghenescu, A. Neagu and M. Potlog

Joint Institute for Nuclear Research, Dubna, Russia
A. Zhemchugov, M. Gostkin, A. Rymbekova and A. Maltsev

Université Paris-Saclay, CNRS/IN2P3, IJCLab, Orsay, France
R. Pöschl

School of Physics & Astronomy, Tel Aviv University, Tel Aviv, Israel
H. Abramowicz, Y. Benhammou, M. Elad, D. Horn, S. Huang, A. Levy and I. Levy[2]

Tomsk State University, Tomsk, Russia
O. Tolbanov, A. Tyazhev, M. Skakunov, A. Vinnik and A. Zarubin

13 February 2022

[1]also at RWTH Aachen University, Aachen, and Brandenburg University of Technology Cottbus, Germany

[2]also Nuclear Research Centre Negev

Contents

Summary

The electromagnetic calorimeters of the LUXE experiment are designed as sampling calorimeters using GaAs or silicon sensors and tungsten absorber plates. They will measure the number of positrons and their energy spectrum in e-laser and γ-laser interactions (ECAL-P with GaAs sensors) or electrons in γ-laser interactions (ECAL-E). In addition, they will be used for the cross-calibration of the energy scale with the tracker. In the following the mechanical structure, the sensors, the Front-End electronics and the DAQ are described. Monte Carlo simulations based on the GEANT4 package are used to estimate the performance of ECAL-P in terms of energy and position resolution, as well as for the reconstruction of the number of positrons impacting the ECAL-P and their energy spectrum. Similar studies for ECAL-E are planned.

---

1 Introduction

The LUXE experiment will explore the uncharted territory of strong field quantum electrodynamics (SFQED) in e-laser and γ-laser interactions at an effective field strength at and above the Schwinger limit. In this regime, non-linear and non-pertubative effects are expected to appear in the production rates of electron-positron pairs. Hence, the number of electron-positron pairs and their energy distribution in e-laser and γ-laser interactions are key characteristics to probe SFQED. In the LUXE experiment, the schematic layouts of which is shown in Fig. ref:layoutdetailed, positrons originating from trident production in e-laser and from the Breit-Wheeler process γ-laser interactions will be measured in a detector system consisting of a tracker followed by an electromagnetic calorimeter, ECAL-P. The ECAL-P design is based on a technology for highly compact electromagnetic calorimeters which was developed by the FCAL collaboration [1, 2], an R&D collaboration to design, build and test prototypes of luminometers for future linear electron-positron colliders, (ILC or CLIC). In the γ-laser setup, also the spectra of electrons originating

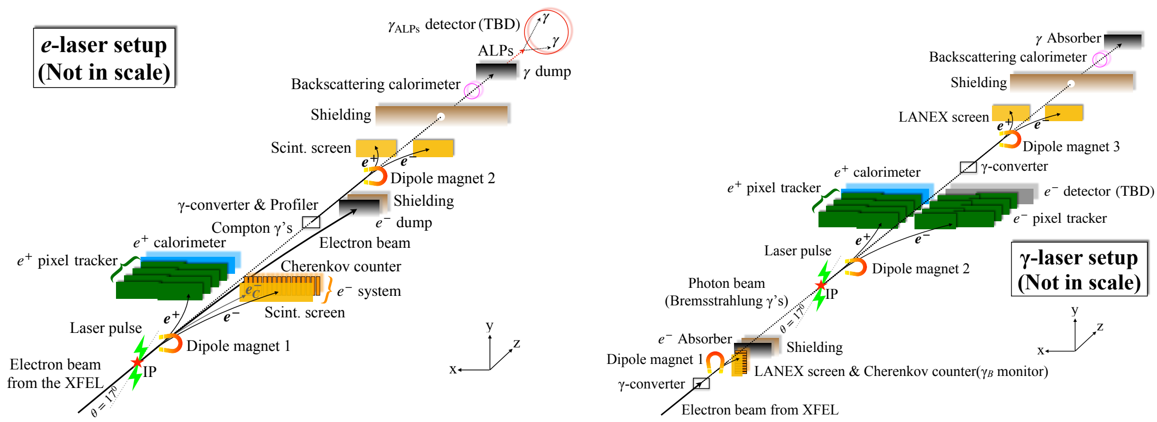

Figure 1: Schematic layouts for the e-laser and γ-laser setup. Shown are the magnets, detectors and main shielding and absorbing elements.

from the Breit-Wheeler process will be measured. For that purpose, the same tracker as for positrons will be followed by the prototype CALICE silicon-tungsten electromagnetic calorimeter, ECAL-E [3]. The highly granular ECAL-E is the reference design of the electromagnetic calorimeter for the International Large Detector (ILD) concept.

The tracker and the ECAL-P (ECAL-E) are located downstream of a dipole magnet which directs the positrons (electrons) from the interaction point to the detectors. The correlation between the position and the energy of the positrons, determined by the dipole magnetic field, constitutes the basis for energy measurements in the tracker. By directly measuring the energy, the ECAL-P can determine whether more than one particle had almost the same path. Thus, the role of the ECAL-P is to determine, independently of the tracker, the number and energy spectra of positrons. The combination will provide an independent in situ energy calibration. In addition, it will ensure a good control of the beam-related background.

In the following the design and performance mainly of the ECAL-P is described in detail. Whenever available, details about the ECAL-E are also provided.

2 Requirements and challenges

To measure the number and energy spectrum of positrons per bunch crossing, challenges and requirements depend on two major scenarios. In the first, when the number of positrons is very small, the showers must be measured on top of low energy, but widely spread, background. In the second, when the number of positrons is large and single positron showers overlap, the number of positrons and their spectrum can still be measured using an energy flow algorithm as explained below. However, non-linearity of the readout electronics and potentially of the signal generation in the sensor has to be taken into account. In the first scenario, a small Molière radius and high granularity will improve the performance of the measurement. In the second, high granularity becomes essential. To get a quantitative picture, a custom-developed strong-field QED computer code, named PTARMIGAN [4], is used to simulate the strong field interactions for the relevant physics processes. Simulations are done for different laser parameters. For phase-0, at the start of the experiment, a laser power of 40 TW is assumed, while in phase-1 the laser power is increased to 350 TW. To achieve different values of ξ, the laser focus is varied. The positron yield per bunch crossing for e-laser and γ-laser interactions are shown in Fig. 2 as function of ξ, where ξ is the intensity parameter of the laser field. It is seen that

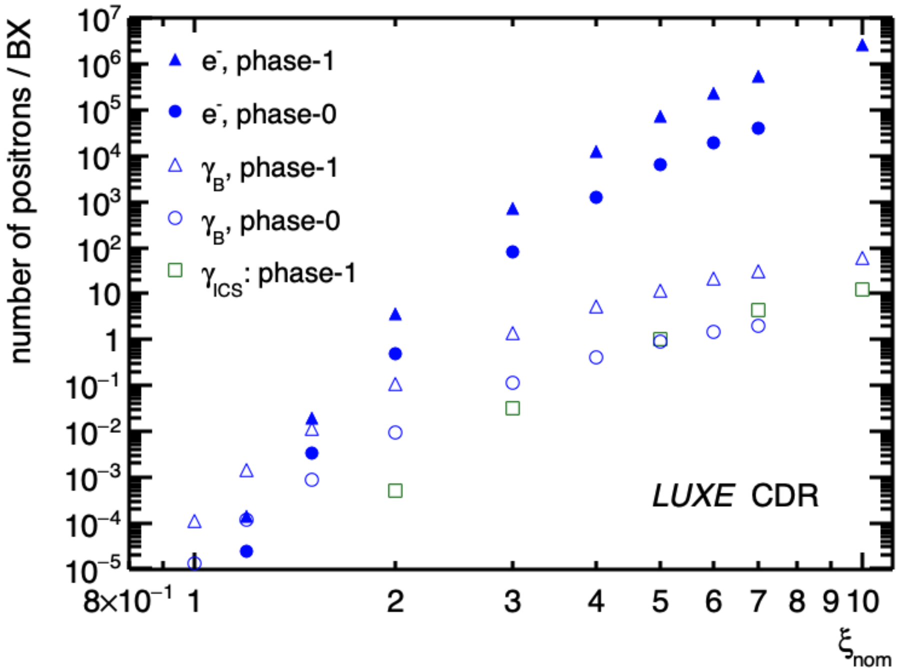

Figure 2: Number of positrons per bunch crossing produced in the e-laser and γ-laser setups for phase-0 and phase-1, as a function of ξ. The electron beam energy is set to 16.5 GeV, and the laser waist parameter varies between 100 μm and 3 μm in the range of ξ.

for the e-laser mode the positron yield is larger than for the γ-laser one by a factor of $\sim 10 - 10000$, depending on ξ. For phase-0 of the e-laser run, up to 10^5 positrons are expected per bunch crossing, while for the γ-laser running at low ξ, most of the bunch crossings are without a positron, and only $\sim 10^2$ are expected at the highest ξ. For phase-1 the rates are roughly 10–100 times larger. [1] The expected positron spectra are typically between 2 and 14 GeV, and are slightly softer for the e-laser mode, as can be seen in Fig. 3.

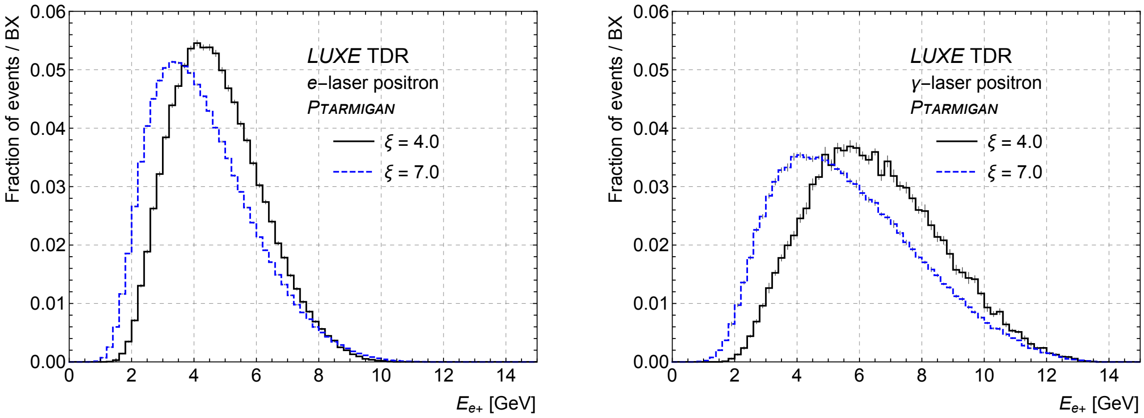

Figure 3: The positron energy spectrum for the e-laser and the γ-laser setup for phase-0 for different values of ξ.

Also shown in Fig. 3 are the expected energy spectra for phase-0 for both processes for selected ξ values. With increasing ξ values, the maximum of the spectrum slighty shifts toward lower energies.
To keep the Molière radius small, a compact sandwich calorimeter with tungsten absorber plates interspersed with solid state pad sensors[2] is designed. The thickness of the tungsten plates is 3.5 mm, corresponding to one radiation length. The gap between two absorber plates is 1 mm, requiring firstly ultra-thin assembled detector planes, and secondly tungsten plates of very good flatness. The acceptance range in the horizontal, x, direction is defined by the positron spectrum and the magnetic field of the dipole magnet, and amounts to about 50 cm. The height in y direction is, due to the small Molière radius, only 5.5 cm.
For performance studies and layout optimisation, full detector simulations are performed using the GEANT4 package. Single positrons with different energies are generated by a gun for basic performance studies. For complex performance estimates, signal and background processes of e-laser and γ-laser interactions are generated with the precursor of PTARMIGAN, IPSTRONG [5].[3]
The ECAL-P is exposed to beam related background. For the electromagnetic component of the background, the expected particle rates and the energy sum of particles impacting the calorimeter per bunch crossing as a function of the x position in the calorimeter are shown in Fig. 4 in the e-laser set-up for the phase-0 laser and $\xi = 3.1$. The background

[1] These numbers can be reduced by defocusing the electron beam.

[2] Simulations are currently performed using silicon sensors. For reasons explained further, the present baseline option is GaAs sensors. The response to relativistic electrons is very similar.

[3] The differences between the two MC generators are mainly in the expected yields but not in the energy spectra and therefore the design of the ECAL-P did not have to be altered.

contribution is split into different particle types and compared to the expected yield of signal positrons.

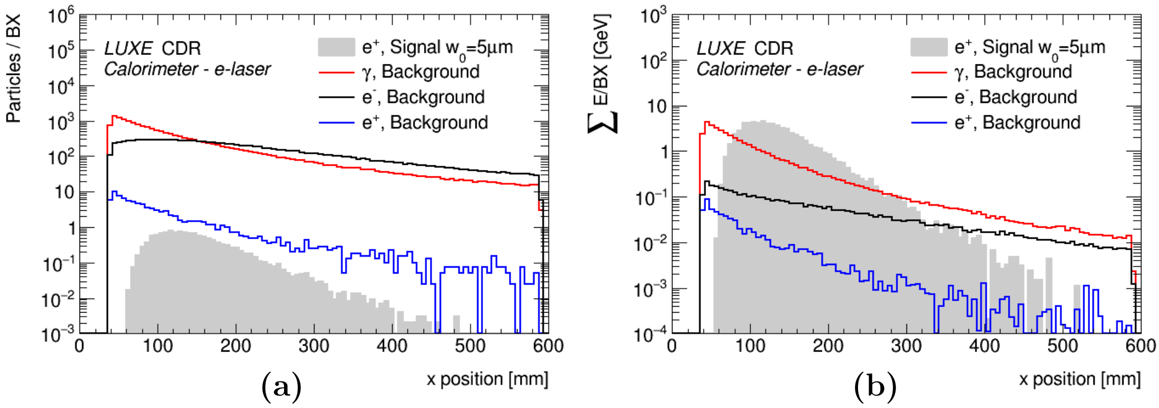

(a) (b)

Figure 4: (a) Number of particles and (b) their energy sum per BX, split into different background particle types and signal positrons as described in the legend, as a function of the x position in the calorimeter for the e-laser set-up for phase-0 and $\xi = 3.1$.

Much of the background originates from a flux of very low energy secondary particles created by the beam, which will be further suppressed by optimization of the vacuum chamber design, the shielding, and the beam-dumps. A new background source was recently identified, originating from the beam-dumps downstream of the ECAL-P, entering from the back of the ECAL. It consists of low energy neutrons. The effect of this background requires further studies with the FLUKA package, more adapted to this purpose, as well as optimization of the beam-dumps design for low neutron back-scattering. Once these studies are completed, extra shielding behind the ECAL for which there is ample space will be considered. This is an ongoing effort. Finally, the irreducible background depositions constitute a signal offset which will be measured in bunch crossings without laser and subsequently subtracted from signal event depositions, pad by pad.

3 System Overview

The LUXE ECAL-P is designed as a sampling calorimeter composed of 20 layers of 3.5 mm ($1X_0$) thick tungsten absorber plates, and assembled sensor planes placed in a 1 mm gap between absorber plates. The whole structure will be held by an aluminum frame, with slots on top to position the front-end boards (FEB). A sketch is shown in Fig. 5.
The ECAL-P is located 4.3 m from the interaction point (IP), 10 cm behind the tracker and 5 cm away from the beam-line on the side towards which the positrons are deflected. A 1 cm thick tungsten plate, extending along the beam-line from the exit of the vacuum chamber, will shield it from the side. The ECAL-P will be installed on a special optical table together with the tracker. From simulation and tests of the LumiCal prototype [2] on which the ECAL-P design is based, the expected energy resolution is $\sigma/E = 20\%/\sqrt{E(GeV)}$ and the position resolution is about 750 μm for electrons of

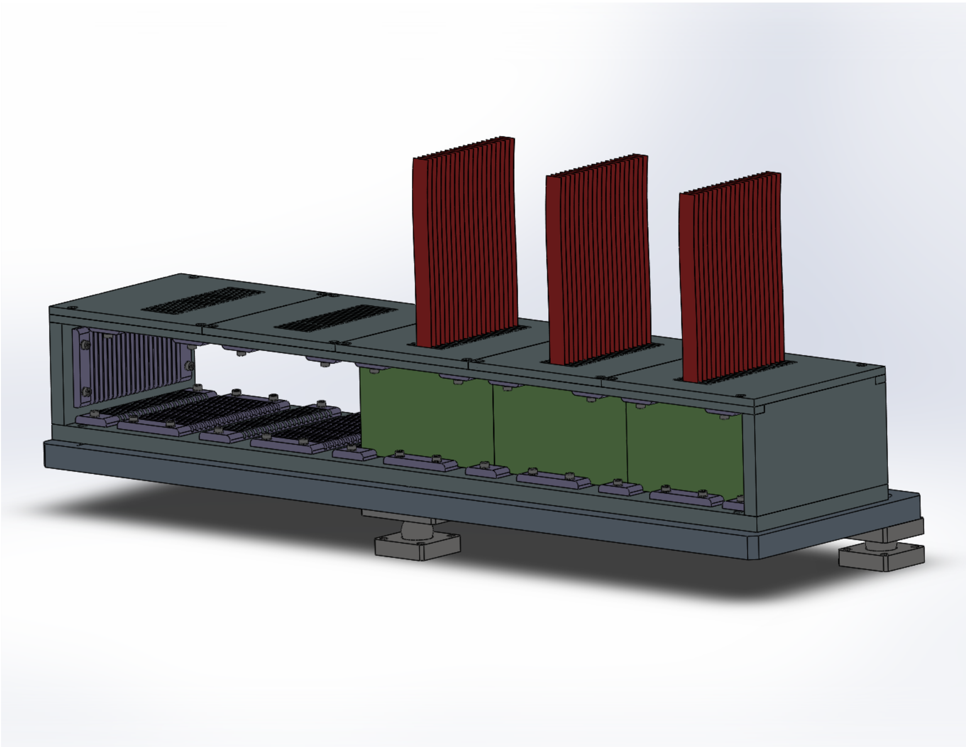

Figure 5: A sketch of the LUXE ECAL-P. The frame holds the tungsten absorber plates, interspersed with assembled sensor planes. The front-end electronics is to be positioned on top of ECAL-P and housed in a cage to avoid pick-up of electromagnetic noise.

5 GeV[4]. The position resolution translates into $\sigma/E = 0.5\%$ to be compared to $\sigma/E = 9\%$ from calorimetry alone.

ECAL-P sensors are made of high resistivity GaAs wafers of 550 μm thickness. Each sensor has a surface of $7.56 \times 5.19\,\mathrm{cm}^2$ and consists of 150 pads. Each complete detector plane will consist of seven adjacent sensors. The fiducial volume of the calorimeter will then be $53 \times 5.2 \times 9\,\mathrm{cm}^3$.

The readout will be based on the FLAME multi-channel readout system [6, 7] which will be adapted for the needs of ECAL-P. The readout of the FEBs will be orchestrated by FPGA boards, connected with cables of a few meters length. The FPGA boards will be located in a rack near the ECAL-P. The FPGAs are connected to a computer via ethernet. The data acquisition and monitoring will be implemented in the EUDAQ system [8]. The power dissipation of the FEBs is estimated to be less than 1 W, hence no active cooling is needed.

For the γ-laser setup, ECAL-E, will be installed behind the tracker on the electron side, "symmetrically" to the ECAL-P. ECAL-E is a sandwich calorimeter with tungsten absorber plates of 2.1 and 4.2 mm thickness, adding up to 9.6 X_0, interspersed with 15 silicon sensors planes.[5] The sensors are structured in pads of $5.5 \times 5.5\,\mathrm{mm}^2$ size (p on n-bulk type), directly connected to SKIROC2 ASICs [9], embedded inside the layer structure. Four $9 \times 9\,\mathrm{cm}^2$ sensors form a sensor layer of 1024 pads, read out by 16 ASICs mounted onto a PCB. The 18×18 cm^2 sensor layer, assembled with ASICs, is called an Active Sensor Unit (ASU).

During 2021 a stack with 15 ASUs, equivalent to 15360 readout channels, has been completed, as shown in Fig. 6.

The total width of the active area of 18 cm of ECAL-E is too narrow to cover the full energy spectrum of electrons and therefore its position will be optimised to cover the maximum of the spectrum, expected around 4 to 6 GeV. However,in 2021 and 2022 more ASUs will be completed, and by the end of 2023 it should be possible to run safely a system that consists of 15 layers of two chained ASUs. The width of ECAL-E will be doubled to 36 cm, thus covering more than 90% of the electron energy spectrum.

4 Expected performance

The performance of the ECAL-P was studied with the LUXE GEANT4 simulation assuming that a sensor plane consist of 320 μm thick silicon sensor, sandwiched between two Kapton layers supported by a thin carbon envelop, with the whole structure having a thickness of 830 μm. The sensors are subdivided in pads of $5 \times 5\,\mathrm{mm}^2$ area. For the current studies, the energy deposited in each pad is used. Signal sharing between pads and signal digitisation will be implemented in the future, based on the results of beam-tests. In the following, we discuss the performance of the ECAL-P for single showers, with and without background, and the expected results for high rates of positrons where single

[4] These values are obtained when the positrons hit the calorimeter under a small angle due to deflection in the dipole magnet.

[5] The stack can be equipped with thicker tungsten plates if necessary. For that purpose a new mechanical structure will be constructed in 2022.

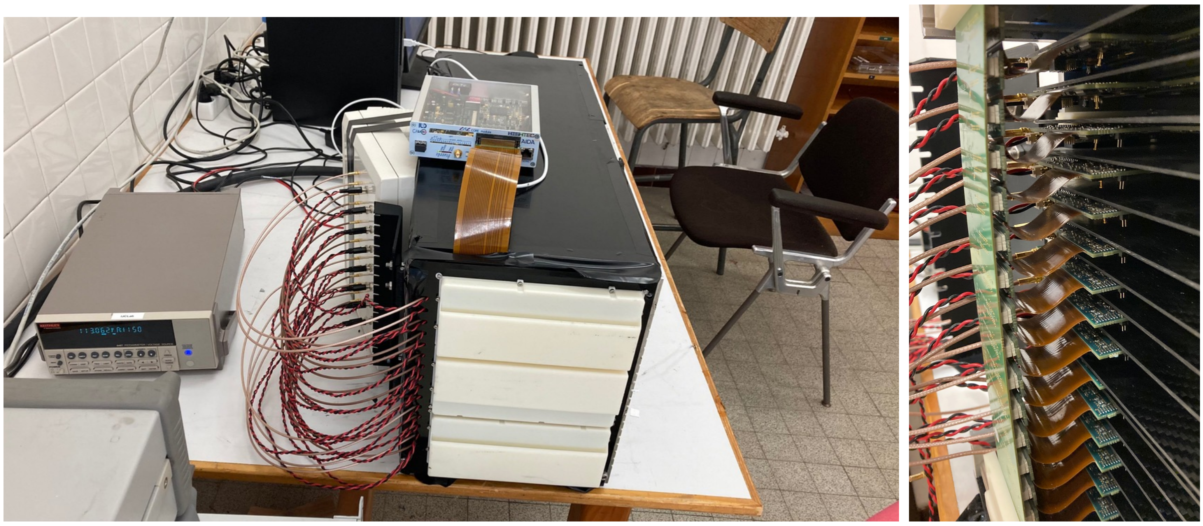

Figure 6: Left: picture of the 15 layer stack of ECAL-E. Visible are the mechanical housing the HV and LV cabling and the flat Kapton cable for the readout of the 15360 pads of the stack. Right: Zoom into the extremities of the stack to appreciate the compactness of the ensemble.

showers cannot be identified and the spectrum is reconstructed through an energy-flow type of approach. The latter case is studied without background implementation. For the medium range rates, we are developing a clustering algorithm which should then lead to a performance similar to the one of single showers.

4.1 Energy and Position Resolution for single positrons

The performance of the ECAL-P for single positrons was studied by generating samples of positrons in the energy (E_0) range between 2 and 15 GeV in steps of 0.5 GeV, assuming the positrons originated from the IP. The positrons enter the calorimeter at an angle due to the deflection in the dipole magnet. After calibration, which takes into account the angular dependence of the response, the dependence of the relative resolution σ/E as a function of the initial positron energy is shown in Fig. 7. A fit of the form $\sim 1/\sqrt{E_0}$ leads to

$$\frac{\sigma_E}{E} = \frac{(20.2 \pm 0.1)\%}{\sqrt{E_0/\mathrm{GeV}}} \,. \tag{1}$$

For the position reconstruction, a logarithmic weighting of the energy deposits in the pads is applied, with a threshold optimised to give the best resolution. Along the y-axis, not affected by the deflection in the dipole magnet, a resolution of $\sigma_y = 460\,\mu$m is achieved. Along the x-axis, $\sigma_x = 550\,\mu$m at 10 GeV is obtained, and a mild dependence on the energy is found. However, while along the y-axis no bias in the position reconstruction is observed, this is not the case for the x position. As shown in Fig. 7, for positrons of 10 GeV, a bias of $\delta x \simeq 500\,\mu$m is generated by the fact that the positrons impact the ECAL-P under a small angle. This is not critical as this bias can be corrected for. An approach based on convoluted neural networks was also applied to the position reconstruction. The resolution (not shown) was not better than for the logarithmic weighting, however there was no bias in the results. The alternative method of determining the energy for single

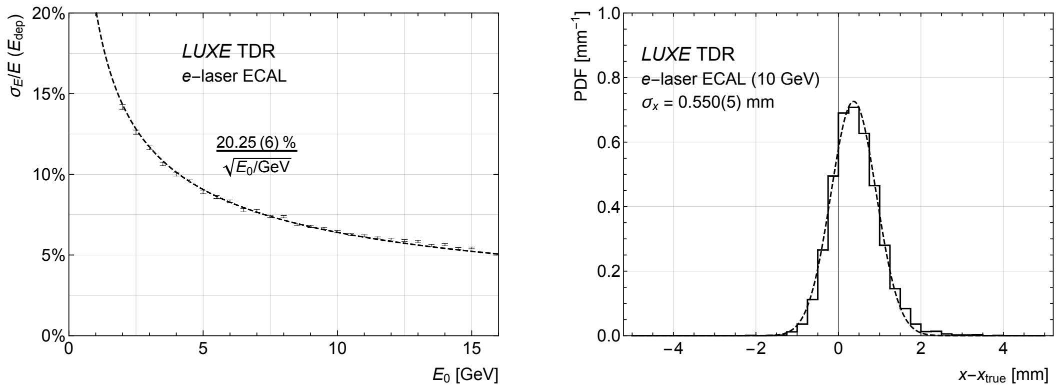

Figure 7: Left: The relative energy resolution of the ECAL-P as a function of the positron energy. Right: The difference between the reconstructed and the generated entry point of the positron shower along the magnetic deflection (x) axis for 10 GeV positrons.

positron showers is by making use of the correlation between energy and position of the positron entry point on the face of the ECAL. The relative energy resolution is then determined by the position resolution. The position resolution as a function of positron energy is shown in Fig. 8. Also shown in the figure is the resulting σ/E compared to the one from calorimetry shown in Fig. 7. Not surprisingly, the σ/E from position reconstruction is better by factor 5 (high energy) to better than 20 (low energy)in the relevant energy range.

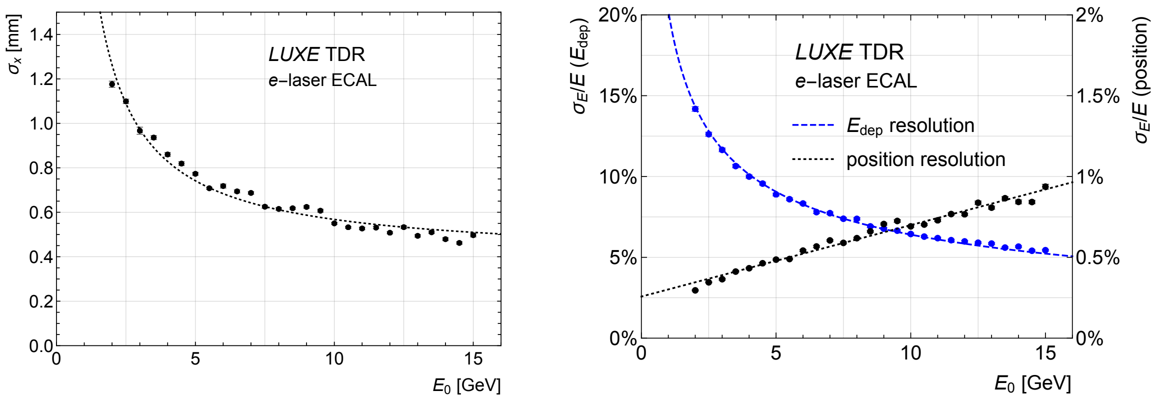

Figure 8: Left: Position resolution as a function of positron energy. Right: The relative energy resolution of the ECAL-P as a function of the positron energy from position reconstruction (right y-scale) compared to the relative resolution from calorimetry (left y-scale).

4.2 Impact of background

It is important to ensure that this performance can also be achieved in the presence of background which is particularly sizable near the beam-line. In this section, we only consider the electromagnetic component of the background. The hadronic component is still under study. The distribution of the background depositions per e-laser bunch crossing is shown in Fig. 9. Also shown in the figure are the depositions for a single positron of 5 GeV. The depositions of the single positron are in a small cone around the

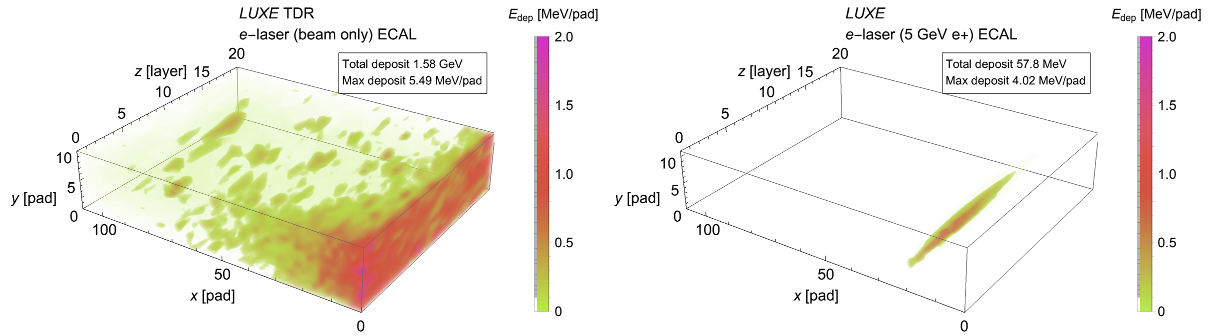

Figure 9: Left: Depositions per bunch-crossing from beam-related background inside the ECAL-P. The beam-pipe is located on the right side. Right: Depositions from a positron of 5 GeV.

shower axis. The background is widely spread and its contribution increases towards the beam-pipe. The effect of this background on the energy deposited in the cone around the shower axis is shown in Fig. 10 for several positron energies. The distribution of the energy deposited by positrons of a given energy is compared to the distribution obtained after adding the background to all pads containing the electromagnetic shower. One clearly observes a shift in the total deposited energy but no significant deterioration in the resolution. As expected, the shift in energy is the more pronounced the higher the energy of the positron, the closer it gets to the beam-line. This is illustrated in Fig. 11 where the ratio between the expected energy deposition with and without background is shown as a function of the positron energy for the e-laser setup. The present estimate of the background contribution is higher than the estimate presented in the CDR (also shown in the figure) because of the change in the window-material at the exit of the vacuum chamber. In the most up to date experimental setup the exit window is made out of aluminum as opposed to Kapton used in the CDR simulations. A similar effect is observed for the γ-laser setup as also shown in Fig. 11. The expected shift in the deposited energy is smaller than in the case of the e-laser setup due to smaller background level. The observed shift in the energy deposited in the ECAL-P due to background can be corrected for by direct background measurements with electron or photon bunches crossing the detector without interaction with a laser pulse, with minimal effect on the resolution for most of the ECAL-P fiducial volume.

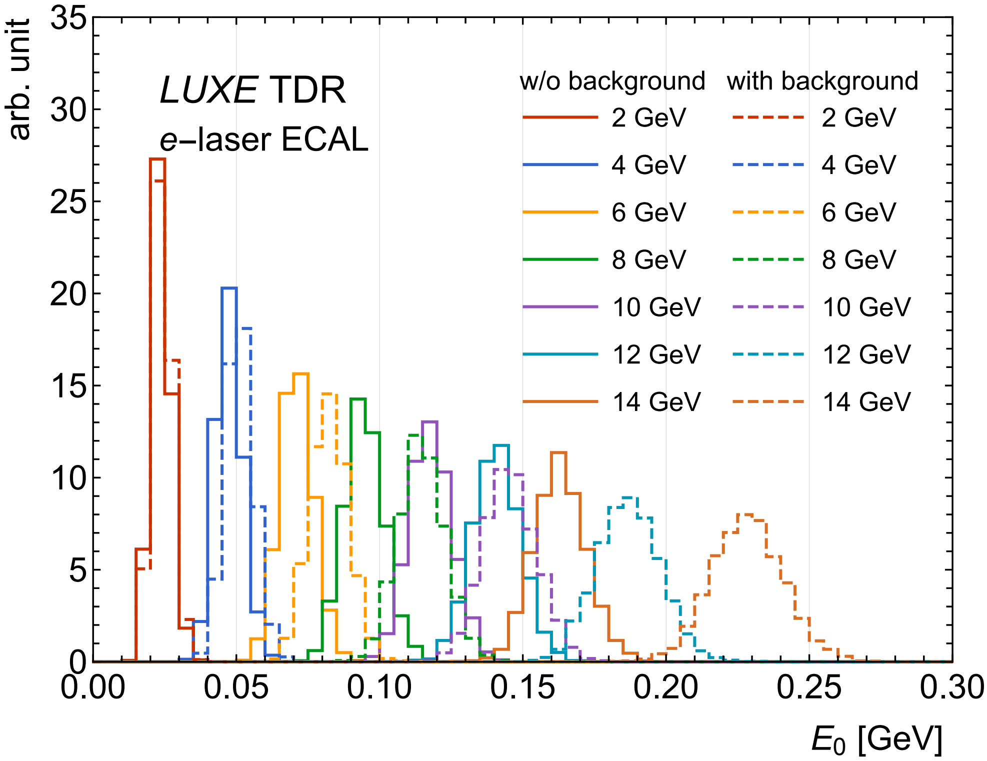

Figure 10: Distribution of total energy deposited in the sensor-pads of the ECAL-P for selected energies of positrons (full lines) and for the same positron showers with added background (dashed-lines) in the e-laser setup. The various energies of the positrons listed in the legend are identified by different colours.

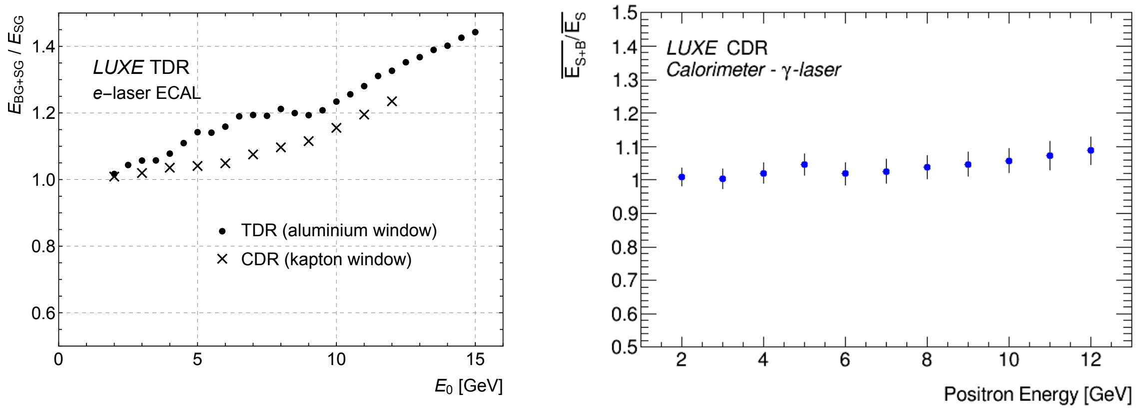

Figure 11: Ratio of the expected energy deposition in the ECAL-P with background to the one without background as a function of positron energy for (Left) e-laser and (Right) γ-laser setups for an aluminum exit-window (TDR) and a Kapton window (CDR). **[SH: The ratio of γ-laser will be corrected later.]** The hadronic background is not included.

4.3 Reconstruction of Positron Number and Spectrum

When the number of positrons entering the ECAL-P becomes large, the showers start overlapping and it becomes impossible to identify individual clusters. Instead a method based on energy-flow is proposed [10], whereby each pad contributes a fraction of the number of positrons in a given energy bin. The latter is determined from the crossing of the path connecting the center of the pad to the IP, according to the dipole magnet field and the geometry, with the face of the ECAL-P, as if the pad was located on the axis of the shower generated by the impinging positron. At the end of this procedure, both the energy spectrum observed in the ECAL-P and the number of positrons (sum over all energy bins) are reconstructed. An overall correction of the order of 2% has to be applied to the reconstructed number of positrons to obtain the number of generated positrons. The relative spread of the number of reconstructed positrons as a function of the number of incident positrons is shown in Fig. 12 (Left). For an average positron multiplicity of about 1000 the projection on the vertical axis is shown in Fig. 12 (Right) . The uncertainty is less than 0.5%. The comparison between the generated and reconstructed

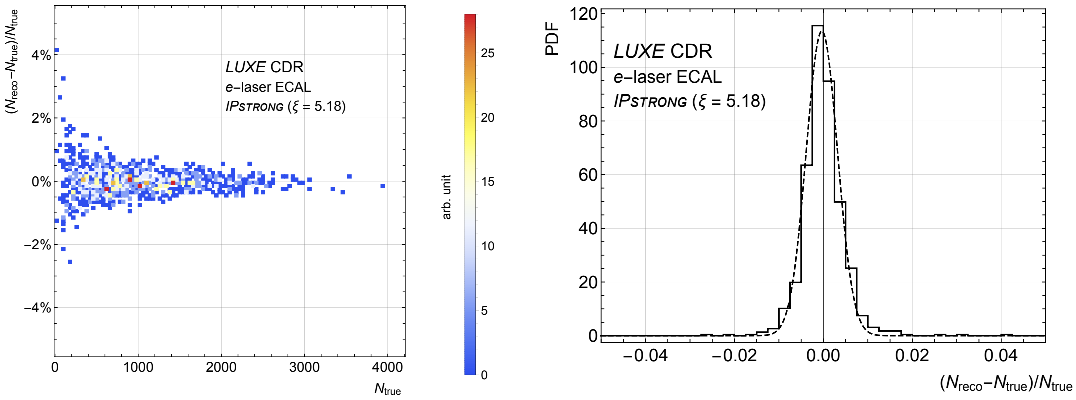

Figure 12: Left: The relative spread of the number of reconstructed positrons as a function of the number of incident positrons. Right: Projection of the relative spread onto the vertical axis for a average positron multiplicity of 1000.

energy spectra is shown in Fig. 13. A good agreement between the two spectra is found, with the exception of the low-energy and high-energy tails, where leakage of the showers sets in. The same reconstruction method was applied to multiplicities of the order of 10^5 (not shown) and still reasonable agreement was found, though the overall correction factor increased to 5%. However, positron multiplicities of this order very likely cannot be measured by the ECAL-P, as they would lead to distortions in the charge drift due high charge density in the sensor and to saturation of the FE ASICs. This problem is under study in order to determine the highest positron multiplicity that can be handled by the ECAL-P. Changing the bunch charge or the electron beam width allows at very large ξ to reduce the number of positrons such that it matches the dynamic range of ECAL-P.
Studies to implement image recognition with convoluted neural networks for the reconstruction of the energy spectra and multiplicities is under investigation. It turns out that with the first 10 layers of the ECAL-P one can already derive the positron multiplicity

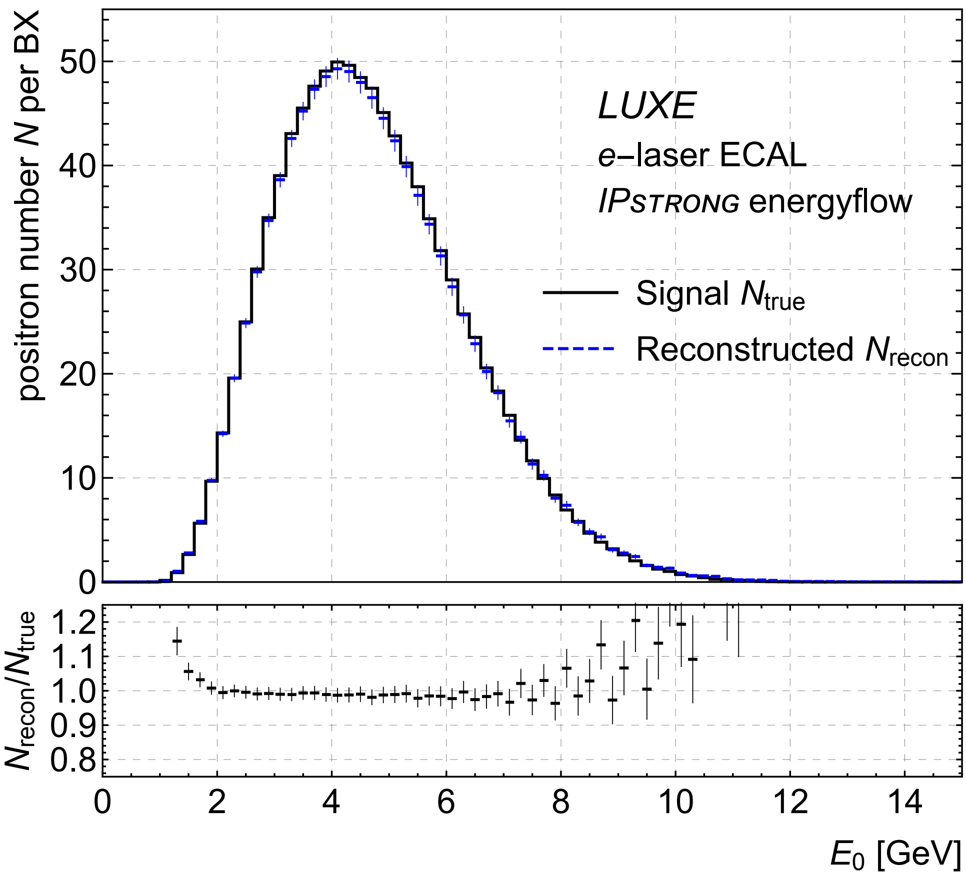

Figure 13: Comparison between the reconstructed and generated energy spectra of the positrons. The ratio of the two spectra as a function of energy is displayed in the lower panel.

and the average energy on an event by event basis. Further studies are underway to reconstruct the full energy spectrum.
The ECAL-E has been introduced only recently into the geometry of LUXE and the study of its performance is underway. However given the similarity between the ECAL-P and ECAL-E in sampling and granularity, similar results are expected.

5 Technical description

In the following subsections the mechanical structure, the sensor options, the structure of the sensor planes, the front-end (FE) electronics and the data acquisition of ECAL-P are described in detail.

5.1 ECAL-P Frame and Tungsten Plates

A frame made of aluminum ensures the mechanical stability of the calorimter and allows the precise positioning of sensor planes and tungsten plates. The frame was manufactured in the workshops of JINR, Dubna. A picture of the frame with four inserted tungsten plates is shown in Fig. 14.

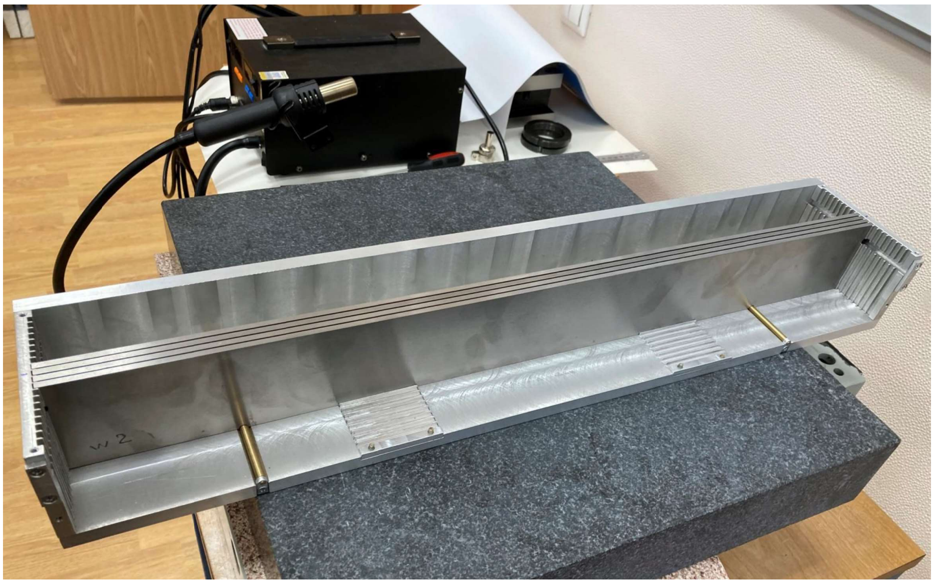

Figure 14: The mechanical frame of ECAL-P with four tungsten plates inserted. The frame is made of aluminum. The bars, made of brass, allow the precise positioning of detector planes and tungsten plates.

The requirement on the mechanical frame is to allow the insertion of 20 tungsten plates of dimensions $556 \times 63 \times 3.5\,\mathrm{mm}^3$, parallel to each other with a gap in-between each two plates equal to 1 mm, with a maximal deviation of $\pm 100\mu$m all over the tungsten plate surface. All materials used must be non-magnetic. The 20 tungsten plates will be moved in very precise aluminum combs, ensuring that the distance in-between plates is equal to the reference distance within $\pm 100\mu$m. In addition, four highly precise brass bars will be used for precise positioning of the plates in the horizontal and vertical directions. Tungsten plates are made of an alloy of 92.5% tungsten, 2.25% copper, 5.25% nickel with density $17.4\,\mathrm{g/cm}^3$.

5.2 Pilot tests of tungsten plates

Four tungsten plates were delivered and measured in JINR. The results of the tickness measurements along the width and height of the plates are shown in Fig. 15. The plate

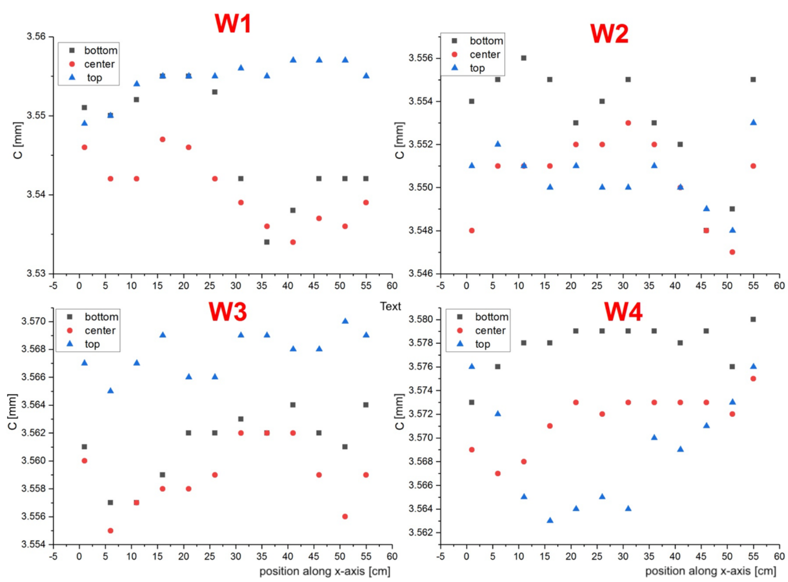

Figure 15: Tickness (C) of four tungsten plates delivered to JINR as a function of the position along the width of the plates (x-axis) measured at the bottom, centre and top of the plates.

thickness is uniform along the surface to within $20\,\mu$m. The plates are thicker than the required 3.5 mm, from $34\,\mu$m up to $80\,\mu$m. The aluminum frame will be modified to allow for this extra thickness. Free plates develop a bending which is removed when installed in the frame comb. Since this issue may affect the gluing of the sensors directly on the tungsten, as planned, further actions with the producer will be undertaken.

5.3 Sensor Options

5.3.1 GaAs Sensors

GaAs sensors are made of single crystals. High resistivity of $10^9\,\Omega$m is reached by compensation with chromium. The pads are $4.7 \times 4.7\,\mathrm{mm}^2$, with 0.3 mm gap between pads. Pads consist of a $0.05\,\mu$m vanadium layer, covered with a $1\,\mu$m aluminum, made with electron beam evaporation and magnetron sputtering. The back-plane is made of nickel and aluminum of 0.02 and $1\,\mu$m thickness, respectively. The sensors are $550\,\mu$m thick with overall sizes of $51.9 \times 75.6\,\mathrm{mm}^2$. The active area is $74.7 \times 49.7\,\mathrm{mm}^2$ leading to 15×10 pads without guard rings. The signals from the pads are routed to bond pads on the top edge of the sensor by aluminum traces implemented on the sensor itself, thus avoiding the presence of a flexible PCB fanout. The traces are made of $1\,\mu$m thick aluminum film deposited on the silicon dioxide passivation layer by means of magnetron sputtering. A prototype sensor is shown in Fig. 16.

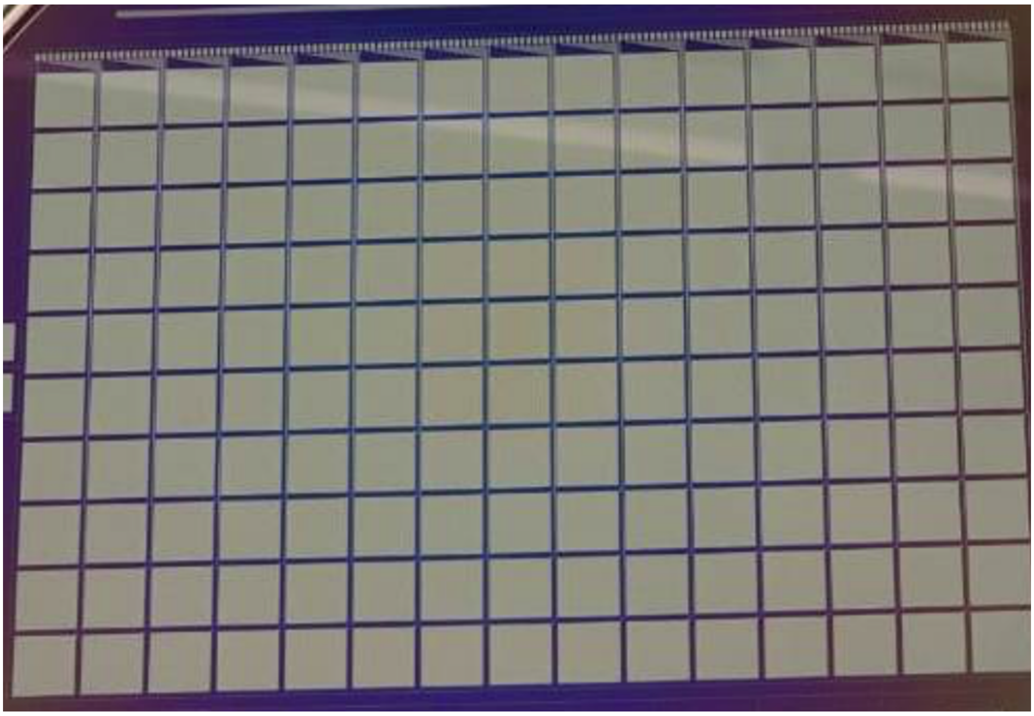

Figure 16: Picture of a GaAs sensor. The bond pads are visible on top of the sensor.

Details on the sensor structure can be seen in the cross-profile shown in Fig. 17.
Using several prototype sensors, the leakage current of all pads was measured as a function of the bias voltage. A typical example is shown in Fig. 18. At a bias voltage of 100 V the leakage current amounts to about 50 nA.
The implementation of the aluminum traces is a new technology, and its performance with respect to cross-talk and noise will be measured in a test-beam. In case the results are not satisfactory, a backup is considered using the flexible PCB fanout as foreseen in the silicon option below.

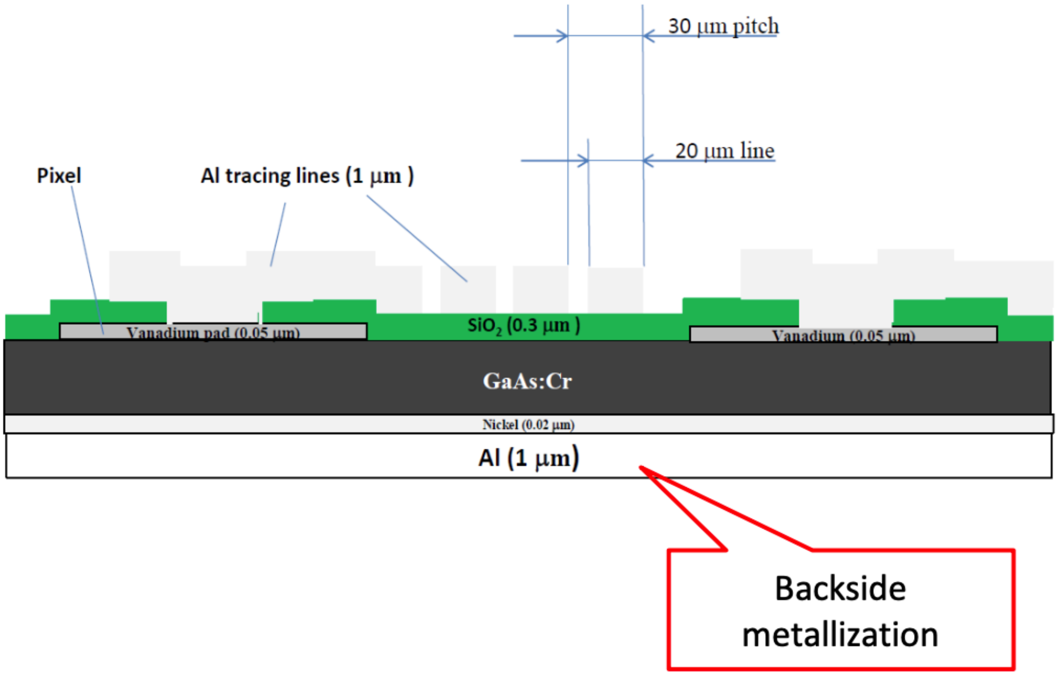

Figure 17: Cross-profile of a GaAs sensor. The aluminum traces are positioned between the pads, on the top of the passivation layer.

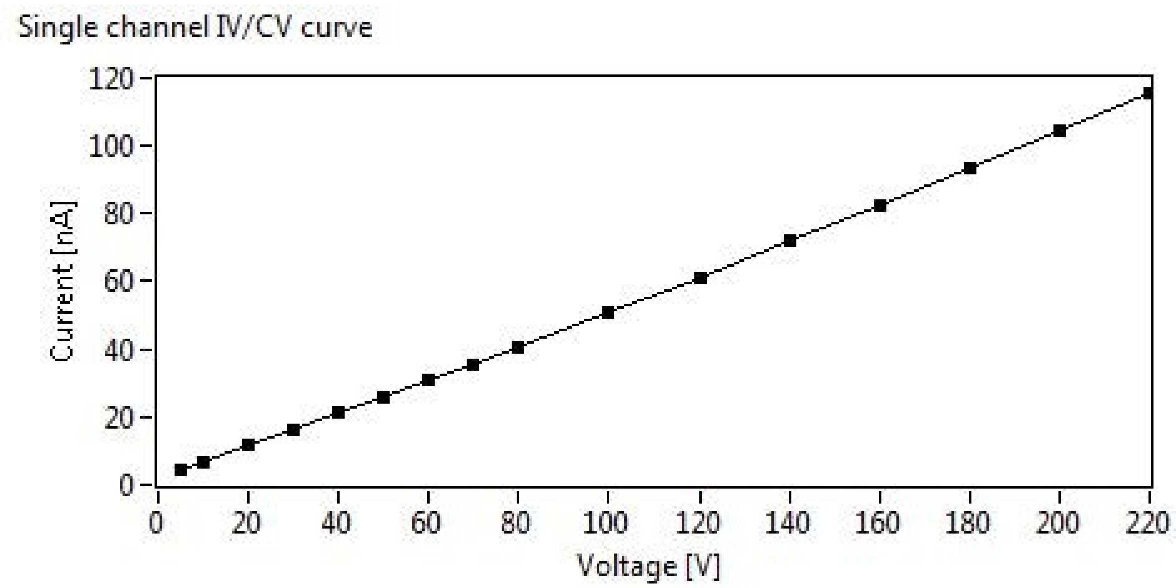

Figure 18: The leakage current of a pad as a function of the bias voltage, measured at 20°C.

5.3.2 Silicon Sensors

The silicon sensors are arrays of $5.5 \times 5.5\,\mathrm{mm}^2$, $p+$ on n substrate diodes made of $320\,\mu$m thick silicon with a resistivity of $3\,\mathrm{k\Omega cm}$, and a reverse bias voltage of about $200\,\mathrm{V}$, without guard rings. Each sensor will have a total area of $89.7 \times 55.3\,\mathrm{mm}^2$, corresponding to 16×10 pads. Sensors of area $89.7 \times 89.7\,\mathrm{mm}^2$ have been produced by Hamamatsu Photonics for the CALICE collaboration, as shown in Fig. 19, and four of them were tested for LUXE purposes.

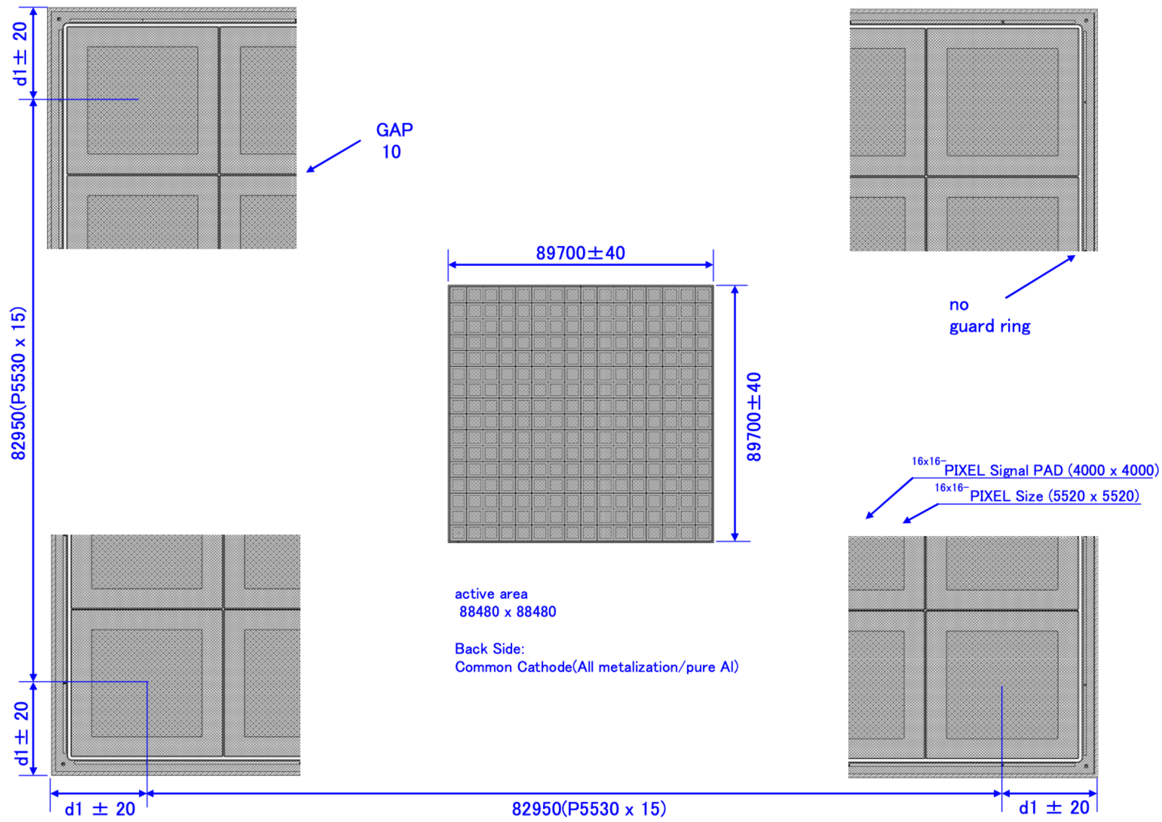

Figure 19: Details of the geometry of the CALICE sensor.

For all pads of the four sensors the leakage current was measured as a function of the bias voltage. A typical result is shown in Fig. 20. In order to route the signal from the pads to the front end board, a flexible PCB has been designed. It will be glued on the silicon sensors with a conductive glue or an anisotropic conductive film. Another flexible PCB has been produced to connect the bias voltage to the sensor back-plane.

5.4 Assembled Detector Plane

Two different versions of an assembled detector plane are still under study. In the first, the signals from the sensor pads are routed to the FE electronics via copper traces on a flexible Kapton foil of $120\,\mu$m thickness. Conductive glue or anisotropic conductive film

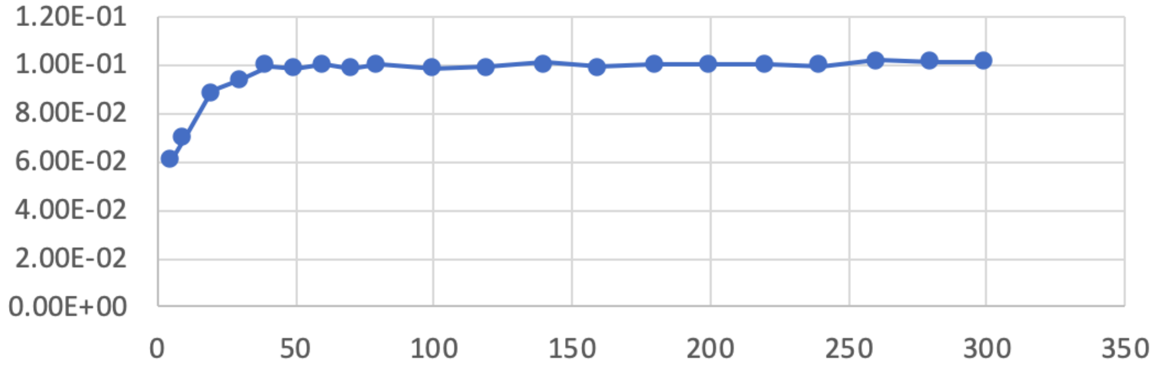

Figure 20: Leakage current (in nA) as a function of the applied voltage (in V) for a selected CALICE pad.

will be used to connect the copper traces to the sensor pads. In the second, thin aluminum traces are embedded directly on the GaAs sensors, routing the signals to the upper side of the sensor. There, integrated bond pads are used to connect the traces to the FE electronics. The bias voltage is in both cases supplied to the back-side of the sensor by a 70 μm flexible Kapton-copper foil, glued to the sensor with a conductive glue.

A sketch of the structure of the detector plane using a Kapton fanout is shown in Fig. 21. A carbon fiber layer is used to protect the sensor but will not be used in the ECAL-P.

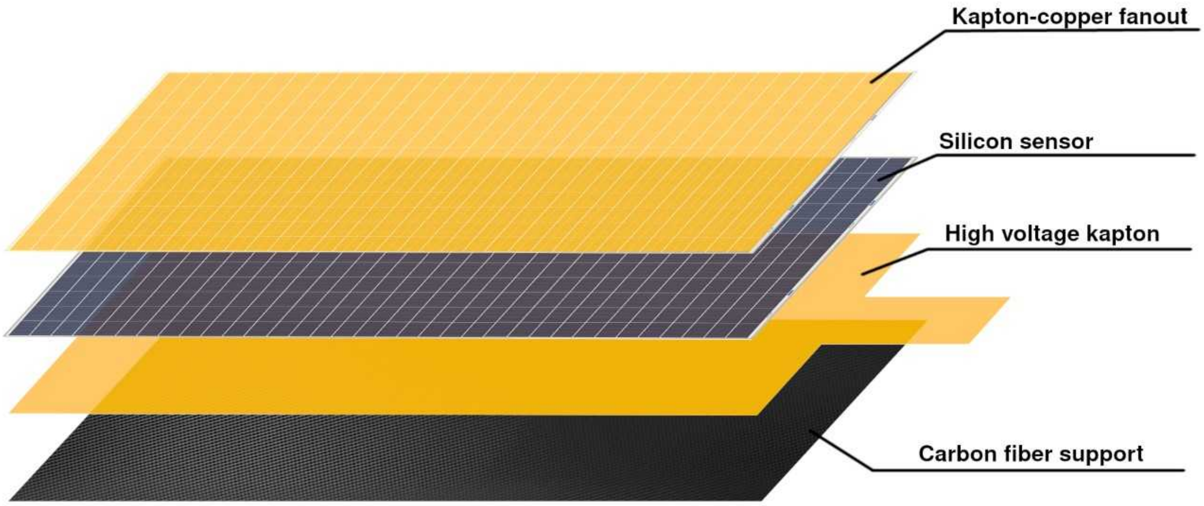

Figure 21: The structure of the assembled detector plane using a Kapton fan-out for the signal routing. The total thickness of the plane is about 650 μm for silicon sensors and 850 μm for GaAs sensors.

5.5 Front-end electronics

Each detector plane will be read out by FE ASICs called FLAXE (**F**ca**L** **A**sic for **X**FEL **E**xperiment), mounted on a PCB, denoted hereafter as front-end board, FEB, and positioned on top of the calorimeter frame. On the side of the FEBs, connectors are foreseen for cables to transfer digital signals from FLAXE ASICs to the FPGAs installed at a larger distance. The FLAXE FE electronics is based on the existing readout ASIC called FLAME (**F**ca**L** **A**sic for **M**ultiplane r**E**adout), designed for silicon-pad detectors of the LumiCal calorimeter for a future electron-positron linear collider experiment. The main specifications of the FLAME ASIC are shown in Table 1. A block diagram of FLAME,

Variable	Specification
Technology	TSMC CMOS 130 nm
Channels per ASIC	32
Power dissipation/channel	$\sim 2\ mW$
Noise	~1000 e^-@10 pF + 50e^-/pF
Dynamic range	Input charge up to $\sim 6pC$
Linearity	Within 5% over dynamic range
Pulse shape	T_{peak} ~55 ns
ADC bits	10 bits
ADC sampling rate	up to $\sim 20\ MSps$
Calibration modes	Analogue test pulses, digital data loading
Output serialiser	serial Gb-link, up to 9 GBit/s
Slow controls interface	I^2C, interface single-ended

Table 1: Summary of the specifications of the FLAME ASIC.

a 32-channel ASIC designed in TSMC CMOS 130 nm technology, is shown in Fig. 22. FLAME comprises an analog front-end and a 10-bit ADC in each channel, followed by a fast data serialiser. It extracts, filters and digitises analogue signals from the sensor, performs fast serialisation and transmits serial output data. As seen in Fig. 22, the 32-channel chip is designed as a pair of two identical 16-channel blocks. Each block has its own serializer and data transmitter so that during operation two fast data streams are continuously sent to an external data acquisition system (DAQ). The biasing circuitry is common to the two 16-channel blocks and is placed in between. Also the slow control block is common and only one in the chip. The analogue front-end consists of a variable gain preamplifier with pole-zero cancellation (PZC) and a fully differential CR–RC shaper with peaking time ~ 55 ns. The shaper includes also an 8-bit DAC, with 32 mV range, for precise baseline setting. The analogue front-end consumes in total $1-1.5$ mW/channel. The ADC digitises with 10-bit resolution and at least 20 MSps sampling rate. The power consumption is below 0.5 mW per channel at 20 MSps. In order to ensure the linearity of the ADC, the input switches are bootstrapped, reducing significantly their dynamic resistance.

The architecture of the FLAXE ASIC will be very similar to the existing FLAME design. In particular the same analog signal processing scheme will be kept. A few modifications

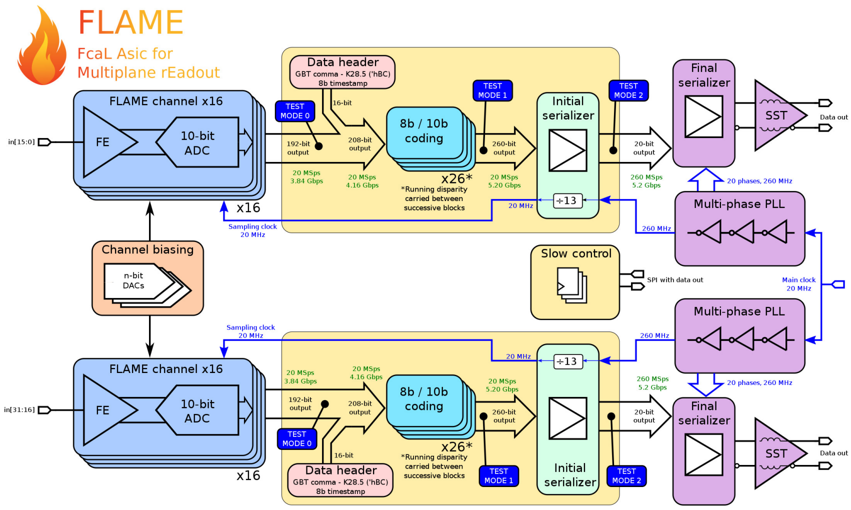

Figure 22: Block diagram of a 32-channel FLAME ASIC

are needed, mainly in the digital part. The fast data transmission components will be replaced by a simpler and slower data transmitter to reduce the complexity and the cost of the subsequent FPGA-based back-end and DAQ system. This is possible, since the data rate and data volume in LUXE is much less than for LumiCal. Depending on the sensor type which will be used in the experiment, small adjustments in analog front-end, e.g. charge-to-voltage gain, may also be needed. The dynamic range of the ASICs can be switched between high and low gain. At high gain the response to the input charge is almost linear between deposition from 0.5 to 75 minimum-ionising-particle (MIP) equivalent. At low gain the charge at the preamplifier input is limited to 5 pC, corresponding to about 10000 MIP-equivalent, and the lower threshold is in the range of a few 10 MIP-equivalent.

The power dissipation of the FE electronics amounts to a maximum value of about 50 W. However, it can be reduced by roughly a factor 10^3 by power pulsing, foreseen for application in LUXE. Hence for normal operation, cooling will not be needed. However, for calibration and alignment it is planned to take data with cosmic muons. For this case dedicated air cooling of the FEBs will be foreseen.

6 Interfaces and Integration

6.1 Trigger

For the normal operation of ECAL-P, the trigger will be provided by the Trigger Logic Unit (TLU), as shown in Fig. 23 and described in detail in the LUXE DAQ technical note [11].

The TLU will distribute to all the sub-detectors the trigger signal coming from

- the electron beam with a frequency of 10 Hz,

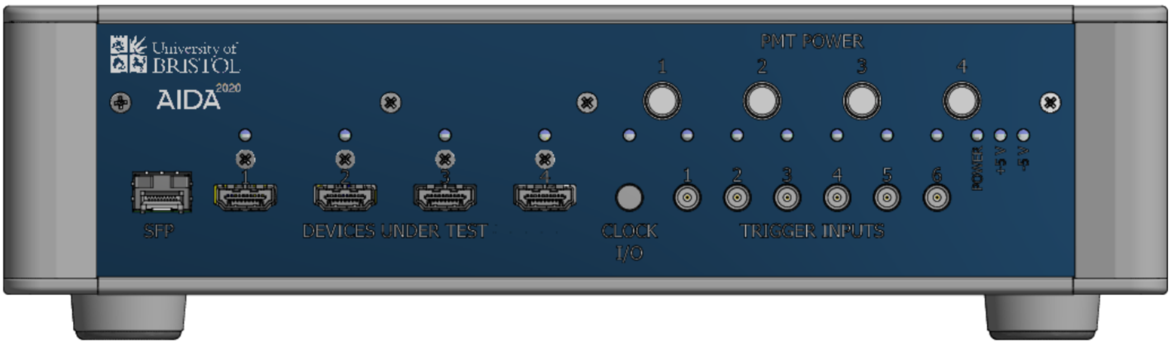

Figure 23: Front view of the TLU.

- the laser beam with a frequency of 1 Hz.

The trigger signal will be sent to the FPGA-based back-end, which will then distribute it to the FLAXE ASICs located at the ECAL-P FEBs via dedicated differential links. The FPGA will perform a programmable phase shift of the trigger signal in order to wake up the FLAXE ASICs just before the next bunch crossing using the power pulsing feature. Effectively, the FPGA will use the trigger originating from a particular bunch crossing to predict the next one, to start the analogue and the mixed-mode signal processing, as well as the data acquisition in the FLAXE ASICs. The ASICs will remain active, writing the data into an internal memory, in a time window sufficient to fully collect the bunch crossing event. After this time, the analogue and mixed-mode signal processing part of the FLAXE ASICs will be automatically switched off, and data collection will be stopped. The collected event will be held in the internal FLAXE ASICs memory and successively read out by the FPGA between bunch crossings.
During the construction of the ECAL-P at DESY, a cosmic muon trigger will be installed. It will consist of two scintillators and PMTs, connected to NIM modules to create the logic. This will provide an asynchronous trigger to the FPGA-based back-end, which will be distributed the same way as the synchronous trigger, only without the phase shift. The FLAXE ASICs will run continuously, processing and collecting the data into the circular buffer in the internal memory integrated into the ASICs. The asynchronous trigger will then stop the data collection in the ASICs, allowing the FPGA to read out the cosmic muon event. The data collecting process will restart automatically as soon as the event data is read out by the FPGA.

6.2 Data Acquisition

The seven GaAs, or six silicon, detector planes in each ECAL-P layer will be equipped with a single FEB, common for all sensors in the layer. All FLAXE ASICs on a FEB will be connected in parallel to the common data bus. The data bus will use a SPI-like, synchronous, serial protocol in the physical layer, with three differential links for the bus clock, a serial CLock, SCLK in the range 20 – 60 MHz. Commands are send from FPGA to the ASIC in the regime 'Master Output'–'Slave Input', MOSI, and data from ASIC to

the FPGA as 'Master In'–'Slave Output', MISO. However, in the logical layer, the bus will implement a I2C-like protocol, allowing the FPGA to address and communicate with each ASIC independently. The event data from a single ECAL-P layer will be read out from the FLAXE ASICs sequentially, one ASIC after the other. This bus, on top of the data acquisition, will also serve the slow control and the configuration interface to the ASICs.
Up to the 128 raw ADC samples will be collected in an event for each of the readout channels. With about 1000 channels per single ECAL-P layer and a 10 bit ADC resolution the event size amounts up to 1 Mb. With 10 Hz of bunch crossing rate, this results to about 10 Mb of data per second read out from a single FEB. Therefore the 20 MHz bus clock frequency provides a sufficient bandwidth for a regular operation. A higher bus clock frequency is foreseen for the data acquisition of the asynchronous muon calibration mode, in order to reduce the dead time of the system.
The data from each FEB will be sent to the FPGA board. Since only three, relatively slow, differential links are needed for a single FEB, the data of the whole ECAL-P can be read out and processed by a single FPGA. The signals from the FEBs are fully digital, hence the FPGA board can be positioned at a larger distance from the calorimeter, e.g. in the calorimeter rack. The FEBs will be read out in parallel via different links. Hence, the bandwidth which is sufficient to read out a single FEB will also be sufficient to read the whole ECAL-P between consecutive bunch crossings.
The event will be processed by the FPGA. The signal reconstruction comprises the calculation of the deposited charge and the Time Of Arrival, TOA, from the collection of the raw ADC samples in a given channel. This procedure, combined with zero suppression, will significantly reduce the data rate. Finally the remaining event data will be sent from the FPGA board to the DAQ computer using the User Datagram Protocol, UDP, through a single 1 Gbps Ethernet link. In parallel, the Transmission Control Protocol, TCP, over the same link will be used for the system control and monitoring.

7 Installation, commissioning and calibration

7.1 Detector assembly

The ECAL-P assembly requires the presence of participants from three laboratories engaged in building the ECAL-P:

- JINR - for the mechanical frame and the tungsten plates.
- TAU - for gluing the sensor planes on the tungsten plates.
- AGH-UST - for installing the readout electronics.
- ISS - for software support and slow control.

The assembly will take place at DESY.
The tasks to be performed are then

- Gluing the sensor planes on the tungsten, plate by plate.

- Connecting the FEBs and the electronics.
- Performing a cosmic run for function tests of components.

It is assumed that it will take two days to instrument one tungsten plate and perform the function tests. The gluing will take one day and the glue will be curing during the night. The next day, the instrumented tungsten plate will be inserted into the mechanical frame followed by cabling and connection of FEBs, HV and LV as well as DAQ. After performing a noise check, data from cosmics will be collected during the night. This cycle will be repeated for the 20 plates. It will thus take 40 days to complete these tasks. This will be followed by a full system test for about 10 days. Another 10 days will be needed to perform the ECAL-P calibration in the DESY test-beam. The full assembly is thus expected to take 2 months. With an added contingency to solve unforeseen problems, the total time estimate for ECAL-P readiness to be moved into the experiment is thus three months.
During the phase of the construction of the ECAL-P, the DAQ should be able to work in a standalone mode with a cosmic trigger. For the latter, two scintillators with PMTs and one NIM crate with a trigger based on NIM modules will be provided. Once the ECAL-P is fully tested, the whole system is moved to the pit and the DAQ PC of ECAL-P will be included in the central LUXE DAQ.
The ECAL-E will be fully assembled and tested at LAL Orsay and shipped to DESY. After arrival a system test will be performed and the status of all components will be documented. The time foreseen is one week.

7.2 Installation

For the final installation in the experimental area, it is assumed that:

- the table on which the ECAL-P is placed is installed;
- all LV, HV and data cables are layed out to connect the ECAL-P subsystems with the rack.

The installation steps, with the estimated duration and the number of participants, are as follows:

- Moving the ECAL-P to the area and place it on the table. The rough weight estimate is 50 kg and thus a crane will be needed.
  Duration: 1 day;
  Person power: 1 technician (DESY), 2 physicists.
- Moving the electronics racks to the area next to the ECAL-P (time and person-power included in the previous item).
- Performing the survey, to precisely define the position of ECAL-P;
  Duration: 1/2 day;
  Person-power: experts from DESY/XFEL survey, 1 physicist.

- Connecting the cables between ECAL-P and the rack.
  Duration: 1 day;
  Person power: 1 electronic engineer, 1 technician, 1 physicist.

- Testing of HV, LV and data connections. Duration: 1 day plus 2 days in reserve for potential replacements;
  Person-power: 1 electronics engineer, 2 physicists.

Hence for the installation of the ECAL-P in the area between 3.5 to 5 days are needed. The process will be performed by 2 physicists, 1 electronic engineer and 1 technician (partly provided by DESY), and the DESY survey team. A summary is given in the resource loaded schedule in appendix A.
The installation of the ECAL-E will follow a similar scheme, and performed by members of the CALICE collaboration.

7.3 Commissioning

After installation, the full system test will be repeated. Low voltage settings and currents drawn by the sensors and the FE ASICs will be checked. Pedestal data will be collected with a special trigger, and the pedestal values and width monitored, as a proof of stability and readiness for operation.

7.4 Calibration Strategy

The ECALs will be calibrated in electron beams of precisely known energy. The electron-beam energy available at DESY is limited to 6 GeV. The positron/electron energy range expected in LUXE for Breit-Wheeler type of processes extends to about 15 GeV. Therefore beam-tests at CERN will be required.
To save time and minimise the risks of mechanical damage to the ECAL-P, the following strategy will be adopted. The existing FCAL tungsten prototype mechanical structure will be equipped with 20 sensor planes and FLAXE readout boards. It will then be tested and calibrated in the DESY and CERN test-beams. This will allow to develop the proper MC simulation with digitisation within Geant4. The full ECAL-P will be exposed to the DESY test-beam and the comparison between the results obtained with the FCAL prototype and the ECAL-P at low electron energy will then be used to project the performance of the full ECAL-P at higher electron beam energies. This approach provides more flexibility in the access to test-beams.
Tuning of the calibration after installation will be done in special runs foreseen in LUXE using a photon beam. A needle will be inserted near the IP to convert photons to electron-positron pairs. These pairs will be used to calibrate the tracker energy by imposing the constraint that the invariant mass of the pair has to be zero. The "calibrated" tracks will then be used to cross-calibrate the ECAL-P. The expected energy resolution of the tracker is within factor two the same as the one of the calorimeter when deduced from position reconstruction.
The ECAL-E will be calibrated in the same test-beams and with converted electron-positron pairs as used for the ECAL-P.

7.5 Decommissioning

The decommissioning of the ECAL-P will be done by the laboratories having developed and built the ECAL-P, i.e. the AGH-UST Cracow, the ISS Bukharest, the JINR Dubna, the Tel Aviv University, and the Tomsk State University, and the decommissioning of the ECAL-E will be done by CALICE. The decision about a potential further use of the ECAL-P, or its dismantling, will be decided by the involved parties before the completion of the LUXE the experiment. In case of dismantling, each laboratory will take back the delivered components. The time needed for decommissioning depends on a potential activation of the material, e.g. near the beam line. About a potential intermediate storage at DESY, the parties will propose an agreement with DESY.

8 ORAMS: Operability, Reliability, Availability , Maintainability and Safety

The number of readout channels of ECAL-P and ECAL-E is about 25000, orchestrated by FPGAs. Since the readout frequency during normal data taking is 10 Hz, there should be no problem with the speed of readout and data transfer. The radiation dose for sensors and FE electronics is below a critical level, hence radiation damage is not expected. Solid state sensors are devices of high reliability. There will be no danger of over-voltage break-through or sparks. The change of the leakage current due to temperature changes will be kept small by air conditioning in the area, with a maximum temperature drift of a few °C. The ECAL-P and ECAL-E are modular. In case of malfunctioning of a detector plane it can be replaced by a spare part within a few days of access. For the replacement of faulty FE ASICs or FPGAs, less than a day will be needed. The same holds for the Low Voltage and High Voltage power supplies. The bias voltage for the sensors will be around 100 V. High Voltage connectors and cables will be used, matching the safety requirements.

9 Project Organisation

9.1 Human and financial resources

The LUXE ECAL-P will be built in a joint effort of the AGH-University of Technology (AGH-UST) Cracow, the Institute of Space Science (ISS) Bucharest, the Joint Institute of Nuclear Research (JINR) Dubna, the Tel Aviv University (TAU), and the Tomsk State University (TSU). These institutes will provide the human and financial resources needed for the design, production, test, commissioning and operation of ECAL-P. The group of AGH-UST comprises 5 experienced researchers, specialised in ASIC design, 1 technician and several students. From the ISS group, 3 physicists experienced in software and data handling are included. In JINR, two hardware experts took over the responsibility for the mechanics. In addition, JINR contributes with engineering person-power and workshop infrastructure. The TAU group comprises 3 experienced physicists, 1 part-time technician (full time technician will be hired in the near future), one postdoc, and several under-graduate students. The TSU is specialised in GaAs sensor technology. Currently 3 physicists are contributing to ECAL-P.

The cost estimate for the production of ECAL-P is given in Table 2. The major cost

Table 2: Cost estimates for the various components. The comment discusses the source of the price and its uncertainty where possible.

Component	Cost (kEur)	Origin of estimates	Quality factor	Status
Mechanics	37.8	JINR, CERN	1	Ready
Sensors	160	TSU	1	Prototyping
FE ASICs	165	AGH-UST, from recent submissions	2	Redesign
PCBs	22	AGH-UST and TAU, previous prod.	1	
DAQ	27	FCAL experience	1	
Power supplies	20	current offers	1	
Tooling	30	estimated by TAU	1	
Auxiliary components	30	experience from previous projects		
Total sum	491.8			

drivers are the sensors and the FE ASICs. Compared to the CDR estimates, the price for sensors increased by factor two. The main reason is that no other current project in production stage has silicon sensors that fit the ECAL-P design, which could have substantially reduced the price. The price offer from Hamamatsu, the only producer of silicon sensors on the market, would quadruple the price assumed in the CDR. Compared to that offer, moving to GaAs sensors reduces the price by factor two. In addition, the sensor costs will be shared by TAU and TSU. TAU received support from the PAZY Foundation (Israel Atomic Energy Commission) and has applied for support from the Israel Science Foundation. TSU will use resources from the university.

Compared to the CDR, the estimated price of FE ASICs has increased by about 25% mainly due to expected increased production costs. To cover the costs of the FE ASICs the AGH-UST group has applied for a grant from the Polish National Science Centre. The amount applied for will not be sufficient to cover the increaed cost and further sources of funding will be sought.

The mechanics will be covered from JINR resources, and benefits from the JINR-BMBF program for future detector technologies in the development of tungsten plates of precise thickness and flatness. The DAQ will be part of the AGH-UST application. PCBs, power supplies, tooling and auxiliary components will be shared between AGH-UST and TAU. In addition, TAU together with the DESY group and other participants from Israel and Germany intend to apply to the German-Israeli Project Cooperation (DIP) in the upcoming 2022 call. If successful, some funds will be dedicated to the shortfalls in the ECAL-P funding, if necessary.

At the moment four countries are involved in the CALICE SiW calorimeter prototype effort. These are France, Spain, Japan and Korea. At the moment it can be assumed that the funding in the next two to three years will be continued at the current level in the frame of the base funding for CALICE and Linear Collider activities. The person-power situation is such that there are at the moment around ten senior researchers and engineers, one postdoc, four PhD students and one master student, and the expectation is that the same level of manpower will remain available for the next two or three years. The collaboration between LUXE and CALICE (including the joining of LUXE by CALICE members), a positive development towards a Higgs factory as well as the creation of the French-German lab DMLAB, may lead to an improvement of the situation.

9.2 Schedule and milestones

Currently the ECAL-P calorimeter frame has been produced, sensors are in the prototyping stage and FE ASICs are in the design phase. The schedule for the following steps are shown in Fig. 24. The major milestones ahead are the following:

1. Tungsten plate quality check - July 2022.
2. Sensor performance measurements in test-beam in November 2021, followed by technology choice in February 2022.
3. Completion of the ASIC production in June 2023.
4. Completion of the sensor production in April 2023.
5. Completion of the sensor quality tests in July 2023.
6. Completion of the sensor plane instrumentation in December 2023.
7. Completion of ECAL-P assembly in March 2024.
8. Beam-tests of fully assembled ECAL-P at DESY in May 2024.
9. Readiness for commissioning by July 2024.

The ECAL-E with 15 one-sensor ASUs exits and is currently studied in a test-beam. A second sensor is planned to be added to each ASU, enhancing the coverage in the horizontal direction by a factor of 2. A detailed schedule has to be worked out with the CALICE collaboration.

9.3 Risk management

There are two elements which may impact the time-line and the costs of ECAL-P construction. One pertains to the sensors, the other to the readout delivery.
The technology choice for the sensors boils down to GaAs sensors with or without traces. The November 2021 beam-tests will direct the technology choice. The impact on the costs and the timeline of the ECAL-P is negligible as the sensors are produced by collaborating partners from TSU. The funding is not yet fully guaranteed for TAU. A better assessment will be known in January 2022. The expectation is that if the LUXE project goes ahead,

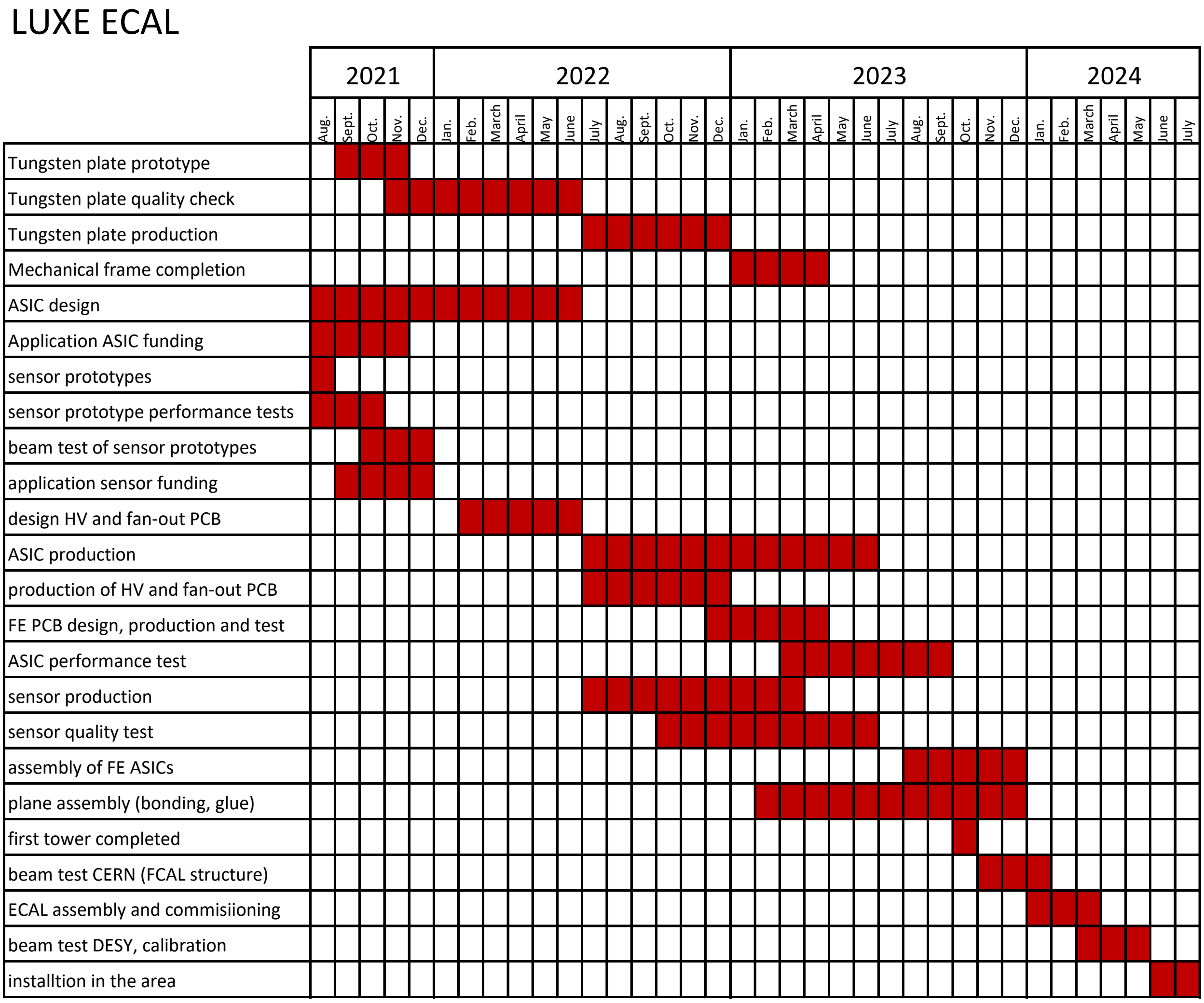

Figure 24: The time schedule for the construction, test and commissioning of the ECAL-P.

shortfalls in funding if any, will be covered by request of extra support from TAU research funds if not by DIP.

The production of the FEB chips is the highest risk enterprise. The main reason is funding, which is not yet guaranteed, and expected delays in chip production which presently affects the whole semiconductor-industry. Time delays of the order of 6 months may be expected. Another factor related to the chip production is an increase in pricing which may be of the order of 25% (included in price estimate). As a mitigating action, the existing FLAME boards will be used for testing purposes. According to the present schedule, that would give an extra 9 months for completing the production and testing of the FLAXE readout boards.

In the worst case scenario, where the lack of funding would prevent the delivery of ECAL-P on time for the phase-0 data taking, the existing ECAL-E will be used on the positron side, leaving the electron side uninstrumented for the γ-laser runs.

An attempt to summarise the risks is presented in Table 3.

Table 3: Risk description, potential impact on cost and schedule, probability to occur and strategy on how to mitigate the risk.

Description	Cost	Schedule	Prob.	Strategy
Sensors GaAs with traces	0	0	30%	Replace by GaAs without traces
FEB chip production	±10%	25% to 35%	30%	Adapt existing FLAME readout

9.4 Responsibilities

Each institute or university will be responsible for a component of ECAL-P, as shown in Table 4. To study the performance of sensors and ECAL-P towers, and finally a

Table 4: The participating institutes and their responsibilities in the ECAL-P construction.

Institute/University	contribution to ECAL-P
AGH-UST	FE-ASICs development and production, DAQ
ISS	slow control, software, computing infrastructure
JINR	mechanical frame, precise tungsten plates
TAU	sensor tests, assembly of detector planes, DAQ
TSU	sensor development and production and test

full system test and calibration, measurements will be done in the test-beam. These campaigns will be organised and funded as a joint effort.

The installation and commissioning of the ECAL-P will again be done in a joint effort, as described in the resource loaded schedule in appendix A.

The ECAL-E is developed by a collaboration of France, Spain, Japan and Korea. France is taking over responsibility for lending, installing, commissioning and operating the ECAL-E within the LUXE experiment.

10 Further tests planned

10.1 Test of components and the whole system in the beam

The current baseline technology for sensors is GaAs made of high-ohmic single crystals with aluminum traces for signal routing integrated in the sensor. This is a new technology, and measurements of the performance are currently done in the laboratory and will be done in the test-beam. Measurements of leakage currents as a function of the applied voltage are done with sensor prototypes and match the requirements, as shown in Section 5.3. Signal size, signal-to-noise and cross talk measurements have been done in the DESY II electron beam end of 2021, and data analysis is just underway. One tower of ECAL-P, comprising 20 detector planes with FLUXE FE ASICs and FPGA read-out, is planned to be fully instrumented in spring 2023. In May 2023 these planes will be used for a calibration at CERN in an electron beam at the PS with electron energies above 5 GeV, followed by a detailed performance study in the DESY II electron beam equal and below 5 GeV in March 2024. Whenever possible, the DAQ of ECAL-P will be integrated into the test-beam EUDAQ system with other LUXE detectors in the test-beam.

The first module of ECAL-E with 15 assembled sensor planes has been just studied at DESY. Similar to the ECAL-P, a beam-test at higher energies at CERN is foreseen. A second test-beam measurement for two-sensor chains will be done, synchronously with the ECAL-P.

For large values of ξ where the multiplicity of positrons may reach up 10^4 particles, there is a risk that the ECAL-P sensors or/and the front-end boards will loose their linear behaviour. The effect of these potentially high charge depositions will be studied in the recently completed DUAL HIGGINS high-power laser facility of Prof. Victor Malka at Weizmann Institute, where up to 10^7 electrons of of $0.7\,\mathrm{GeV}$ (with 5% energy spread) can be produced per laser shot.

Acknowledgements

This study was partly supported by the German-Israeli Foundation under grant no. I-1492-303.7/2019, the Romanian UEFISCDI agency under grant no. 16N/2019, the JINR-BMBF Programme and the Tomsk State University Development Programme («Priority-2030»).

References

[1] H. Abramowicz et al. Forward Instrumentation for ILC Detectors. *JINST*, 5:P12002, 2010.

[2] H. Abramowicz et al. Performance and Molière radius measurements using a compact prototype of LumiCal in an electron test beam. *Eur. Phys. J. C*, 79(7):579, 2019.

[3] K. Kawagoe et al. Beam test performance of the highly granular SiW-ECAL technological prototype for the ILC. *Nucl. Instrum. Meth. A*, 950:162969, 2020.

[4] T. G. Blackburn. https://github.com/tgblackburn/ptarmigan.

[5] Anthony Hartin. personal communication.

[6] S. Kulis, A. Matoga, M. Idzik, K. Swientek, T. Fiutowski, and D. Przyborowski. A general purpose multichannel readout system for radiation detectors. *JINST*, 7:T01004, 2012.

[7] S. Bugiel, R. Dasgupta, M. Firlej, T. Fiutowski, M. Idzik, M. Kopec, J. Moron, and K. Swientek. Ultra-Low Power Fast Multi-Channel 10-Bit ADC ASIC for Readout of Particle Physics Detectors. *IEEE Trans. Nucl. Sci.*, 63(5):2622–2631, 2016.

[8] P. Ahlburg et al. EUDAQ-a data acquisition software framework for common beam telescopes. *JINST*, 15(01):P01038, 2020.

[9] S. Callier, F. Dulucq, C. de La Taille, G. Martin-Chassard, and N. Seguin-Moreau. SKIROC2, front end chip designed to readout the Electromagnetic CALorimeter at the ILC. *JINST*, 6:C12040, 2011.

[10] Mykyta Shchedrolosiev. Optimization of an electromagnetic calorimeter for the luxe experiment. Taras Shevchenko National University of Kyiv, Faculty of Nuclear Physics, 2020. https://agenda.linearcollider.org/event/8107/attachments/34048/55608/main_eng.pdf.

[11] LUXE Collaboration. Technical note on Common aspects.

[12] O. Novgorodova et al. Forward Calorimeters Test Beam Results for Future Linear Colliders. *PoS*, ICHEP2012:552, 2013.

Appendices

A The ECAL plan for the installation

Locations:

- Experimental Area (EA)
- Control Room (CR)

List of components to be installed:

- ECAL detector, including FE PCBs
- HV and LV power supply
- Rack with crates
- FPGA cards
- DAQ Computer with ethernet connection to the rack

Expected installations prior to the one above:

- The optical table for the tracker and ECAL is available and pre-aligned
- Cables for HV and LV between detector table and rack are installed

The details of the resource loaded schedule are shown in Fig. 25.

B Changes since the CDR

Since the CDR, the baseline for the ECAL instrumentation has changed from 320 μm thick silicon sensors to 550 μm thick GaAs sensors. The main reason for this change is that the delivery of the GaAs sensors is guaranteed by Tomsk State University on the time scale required for LUXE. In previous studies [12] it has been demonstrated that the response of GaAs sensors to relativistic particles is similar to that of silicon sensors of comparable thickness. In the sensors to be used for ECAL the only technological change is the implementation of aluminum traces for signal routing to the edge of the sensor. This will make the Kapton PCB with copper traces obsolete, and the critical bonding between copper traces to the sensors pads will be avoided.

	ECAL Installation					
Activity	*Duration*	*Access* *(*) only for extemporaneous interventions*	*ECAL people involved* *PH = Physicist, MEN = Mechanical Engineer, EEN = Electrical Engineer, TE = Technician*	*Man-days*		
Move the ECAL to the Area and place it on the table, move the electronics racks to the area next to the ECAL	1 day	EA	2PH, 1 TE	2		
Survey, to define the position of ECAL precisely	1/2 day	EA	1 PH, 2 survey experts from DESY/XFEL	0.5		
Connecting the cables between ECAL and the rack	1 day	EA	1 PH, 1 EEN, 1TE	1	1	
Tests of HV, LV and data connections;	3 days	EA, CR	2 PH, 1 EEN	6	3	
Test of the readout and standalone DAQ software	3 days	EA, CR	2 PH, 1 EEN	6	3	
Detector calibration	2 days	CR	2 PH	4		
Integartion in the central DAQ	2 days	CR	2 PH	4		
Sum				23.5	7	
FTE years				0.1	0.03	0.01

Figure 25: The resource loaded schedule for the installation of the ECAL. EA stands for experimental area and CR means control room.

C Quality Factor

Table 5: The list of quality factors required for quantification of the level of confidence in a price estimate.

QF1	Off-the-shelf Items for which there is a recent (< 1 year) catalog price or quote with more than one potential supplier Items that are a copy or almost identical to an existing design for which there is a recent (< 1 year) catalog price or quote with more than one potential supplier.
QF2	Items falling short of satisfying a single QF1 criterium, e.g.: - only one potential vendor; - estimate based on not completed design or design with minor modifications; - quotes > 1 year but still sufficiently reliable based on experience.
QF3	Items with quotes > 2 years Items whose cost estimates are based on a conceptual design or adapted from existing design with extensive modifications Items whose costs are estimated using physicist or engineering experience regardless of the maturity of the design.
QF4	Items that have unproven fabrication yields or for which there are unique issues e.g. a special- order item and/or a single preferred supplier.
QF5	Items that are still in a conceptual stage with no detailed specifications or design.

D All notes

This is the list of all notes and the lead editors:

- Technical infrastructure and beam instrumentation at LUXE: Louis Helary and Stewart Boogert
- Laser, interaction chambers and timing system: Matt Zepf et al.
- Laser diagnostics: Matt Zepf et al.
- Common aspects (Simulation, Data Acquisition, Data Quality and Computing): Matthew Wing, Sasha Borysov, Federico Meloni et al.
- Pixel tracker: Noam Tal Hod
- EM calorimeter: Halina Abramowicz and Wolfgang Lohmann
- Scintillation screens: Matthew Wing and John Hallford
- Cherenkov detectors: Ruth Jacobs
- Gamma Profiler: Marco Bruschi
- Gamma Spectrometer: Gianluca Sarri
- Backscattering calorimeter: Maryna Borysova
- physics performance: Beate Heinemann

.... (to be finalized)